Robotica: (2021) volume 39, pp. 1806–1815. © The Author(s), 2021. Published by Cambridge University Press.
doi:10.1017/S0263574720001514

Design and Experiments of Pneumatic Soft Actuators

Liqiang Guo†, Ke Li†*, Guanggui Cheng†, Zhongqiang Zhang†‡, Chu Xu† and Jianning Ding†‡

†*Institute of Intelligent Flexible Mechatronics, Jiangsu University, Zhenjiang 212013, China*
‡*Jiangsu Collaborative Innovation Center of Photovoltaic Science and Engineering, Changzhou 213164, China*

(First published online: February 17, 2021)

SUMMARY
The soft actuator is made of superelastic material and embedded flexible material. In this paper, a kind of soft tube was designed and used to assemble two kinds of pneumatic soft actuators. The experiment and finite element analysis are used to comprehensively analyze and describe the bending, elongation, and torsion deformation of the soft actuator. The results show that the two soft actuators have the best actuation performance when the inner diameter of the soft tube is 4 mm. In addition, when the twisting pitch of the torsional actuator is 24 mm, its torsional performance is optimized. Finally, a device that can be used in the production line was assembled by utilizing those soft actuators, and some operation tasks were completed. This experiment provides some insights for the development of soft actuators with more complex motions in the future.

KEYWORDS: Soft actuator; Gas driving; Superelastic material; Embedded flexible material; Finite element analysis.

1. Introduction

Soft robotic is a rapidly developing research field. It combines robotics with materials chemistry to further advance the development of compliant robotics. Soft robots are basically made of soft materials which makes it light, compliant and safer for human–computer interaction.[1] As an important part of soft robots, soft actuators have various driving methods, such as electroactive polymers,[2–5] shape memory alloys,[6,7] hydrogels[8] and magnetorheological materials.[9] After various stimuli, such as electric charge,[3–7] chemical reaction[10,11] and pressurized fluid,[12–16] the actuator deforms to drive the robot. Most soft actuators are driven by pressurized fluid, which is simpler than other driving methods. When pressurized, the cavity of the soft actuator causes expansion in the direction associated with low stiffness and causes bending,[12,14–16] torsion[16–18] and elongation deformation.[19]

Due to the nonlinear response and the complex geometry of the soft actuator, it is extremely important to accurately predict the performance of the soft actuator (such as the relationship between the pressure of the fluid and the bending, elongation and torsion of the actuator) before fabricating. In recent years, researchers have paid more attention to soft actuators and have conducted limited research work and some applications, such as bionic systems,[20–22] multi-function sports,[13,23] gripping ability,[12,14,23] surgical tools,[24] limb exoskeleton[25] and hand muscle rehabilitation equipment.[26] However, most of these soft actuators can only perform bending deformation in a single direction,[12,14,23] only a few soft actuators are related to torsional actuation[16–18] and other forms of motion are coupled during twisting, resulting in the waste of deformation energy. Besides, the established finite element models (FEM) are all about bending deformation, and there are few FEMs about

* Corresponding author. E-mail: like931212@163.com

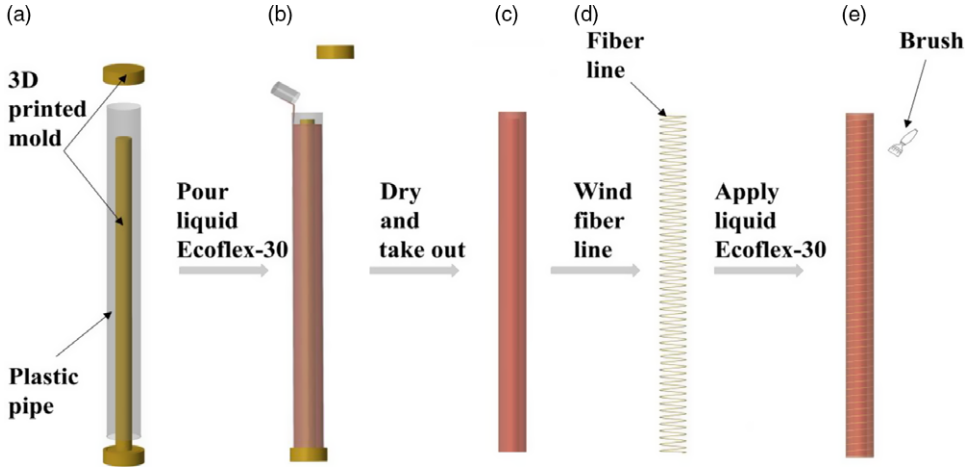

Fig. 1. Soft tube fabrication process. (a) 3D printed mold. (b) Pouring liquid Ecoflex-30 into the mold. (c) Demold the soft tube. (d) Wind fiber line around the surface of the soft tube. (e) Apply liquid Ecoflex-30 to the surface of the soft tube.

torsional actuators. Therefore, it is necessary to design the bending actuator with multi-directional bending deformation and the torsional actuator with pure torsional motion. Similarly, FEMs also need to be established for them.

In this paper, the gas-driven bending actuator and torsional actuator are fabricated by using soft tubes made of super-elastomeric material (Ecoflex-30) and inextensible material (fiber lines). The bending actuator can produce bending deformation in six directions and elongation deformation, while the torsional actuator can produce pure torsional deformation. The FEMs of two actuators are established, and the influence of cavity diameter and other parameters on the performance of the actuator are explored by using established FEMs. The experimental results are compared with the simulation results, and the best structural parameters of the two soft actuators are determined. Finally, by integrating the two actuators, a soft robot arm and soft gripper for the production line are assembled.

2. Fabrication

2.1. Soft tube fabrication

In this experiment, three different types of soft tubes were fabricated, each of which has an outer diameter of 8 mm and an inner diameter of 3, 4 and 5 mm. Specific steps are as follows: firstly, the 3D model of the mold is designed with the help of the Solidworks software and 3D printer. The length of the plastic pipe is 80 mm. Secondly, in a plastic beaker, the two liquids A and B of Ecoflex-30 are mixed in the ratio of 1:1. The mixed liquid is poured into a mold tube and then placed in a vacuuming device for defoaming treatment. After 30 min, it is taken out and put into the drying oven to bake at 65°C for 4 h and, finally, take out the soft tube and wind the fiber lines at equal intervals on the surface of the soft tube (Fig. 1).

2.2. Bending actuator fabrication

Three silica soft tubes of the same specification were selected and placed into the printed support frame. The main function of the support frame is to fix the soft tube to ensure that there will be no relative displacement during the fabrication of the soft actuator. The soft tubes are baked in a drying oven for 30 min after their contact gaps are coated with liquid Ecoflex-30, and then taken them out after solidification. The fabrication process is shown in Fig. 2.

2.3. Torsional actuator fabrication

A rigid plastic tube is placed in the center of the support frame, which is printed by a 3D printer. According to the rotation direction of the support frame, three silicone tubes with the same inner diameter are wound around the rigid plastic tube. After fixing the position, the mixed liquid

https://doi.org/10.1017/S0263574720001514 Published online by Cambridge University Press

Table I. Ecoflex-30 silicone rubber material parameters.

Operable time	Cure time	Elongation at break	Mixed viscosity	Shore hardness	Tensile strength	Tear strength	Shrinkage
45 min	4 h	900%	3000 MPa	00–30	1.379 MPa	68.4 MPa	<0.001%

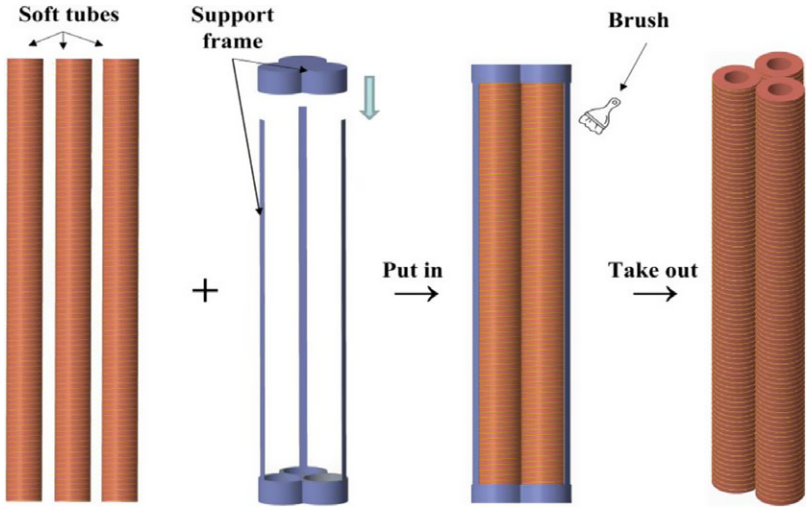

Fig. 2. Fabrication process of the bending actuator.

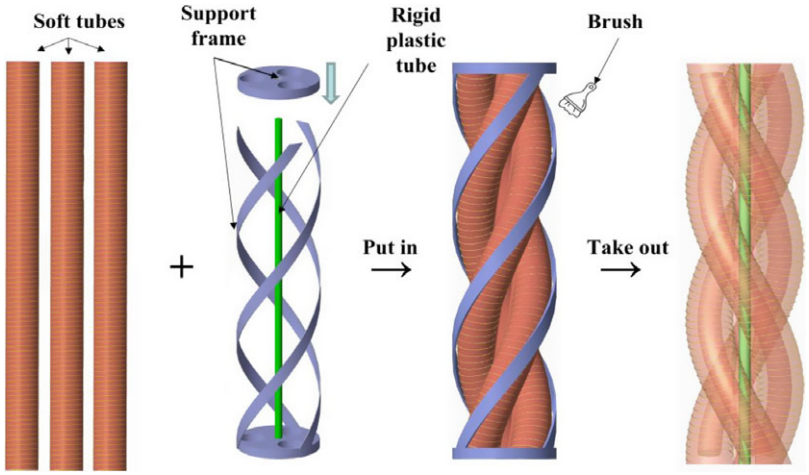

Fig. 3. Fabrication process of the torsional actuator.

Ecoflex-30 is evenly filled between the soft tubes and the rigid plastic tube, and then put the torsional actuator into the drying oven to bake for 30 min. The fabrication process is shown in Fig. 3.

3. Material Properties and FEM Method

The super-elastomeric material Ecoflex-30, fiber lines and rigid plastic tubes are used in the study. These materials are commercially available, easy to use and relatively inexpensive. Ecoflex-30 is a platinum-catalyzed soft rubber. This series of soft rubber is very soft after solidification, has good tensile, tear resistance, good elasticity and elongation and can be restored to its original size after repeated stretching. Table I shows the specific material parameters of Ecoflex-30 silicone rubber.

The FEM analysis that fully captures the behavior of the elastomeric material is very important for reliable and accurate simulation of actuator deformation. The properties of the elastomeric material

https://doi.org/10.1017/S0263574720001514 Published online by Cambridge University Press

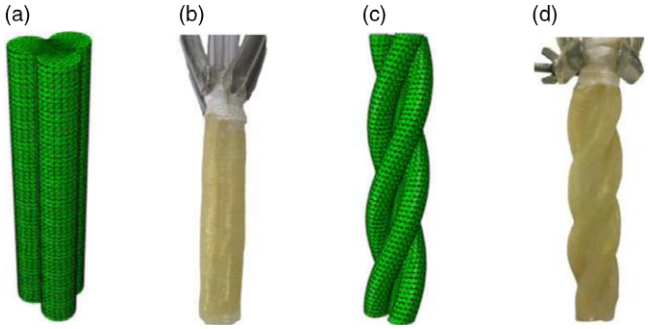

Fig. 4. Finite element analysis model and physical sample of the soft bending actuator (a, b) and the soft torsional actuator (c, d).

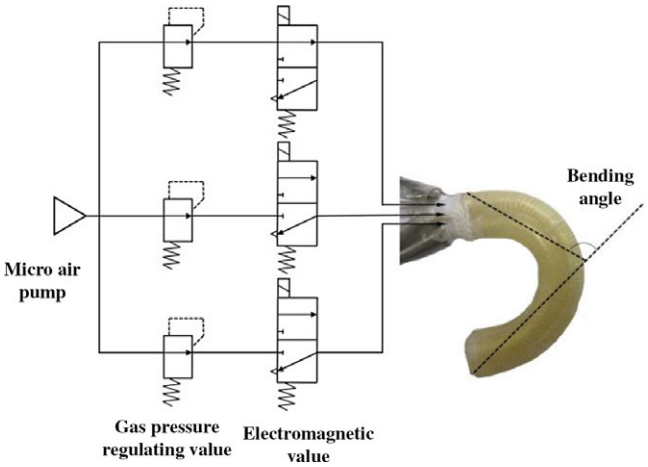

Fig. 5. Connection of each experimental device.

are usually determined by simple testing of small material samples. The main tests are tensile and compression tests in uniaxial, biaxial and planar directions. In order to simulate the highly nonlinear behavior of the soft actuator and select the appropriate superelastic model, the Ecoflex-30 was subjected to a uniaxial tensile test at a speed of 300 mm s^{-1}. After testing the material data, the final model selected for the material is the Ogden model. After optimization, the three parameters of the Ogden model are $\mu_1 = 1.903 \times 10^{-3}$, $\mu_2 = 2.215 \times 10^{-2}$, $\mu_3 = 3.6122 \times 10^{-3}$, $\alpha_1 = -3.855$, $\alpha_2 = 0.6532$, $\alpha_3 = 4.2125$, $D_1 = 3.0587$, $D_2 = D_3 = 0$, where μ and α are the main parameters. All μ terms are in unit of N.mm^{-1} and all D are in unit of N.mm^{-3}.

The FEM analysis is capable of quickly generating actuator response to pressure changes, showing the stress and strain of the actuator and providing a more realistic description of the response to the nonlinear system, giving a better understanding of the effects of local strain on actuator performance. ABAQUS (Simulia, Dassault System) was used to analyze and simulate the behavior of the actuators, and the simplification was reduced to approach the specific experimental conditions. Figure 4 shows the FEMs and physical samples of the two actuators. Because the pressure is directly applied to the inner cavity surface of the actuator, there is no inlet for pressurized air in the FEM of the actuator. The solid tetrahedral quadratic hybrid element was used to model the main body of the actuator. The quadratic beam element was used to model the fiber line, and the fiber line and the actuator were connected by tie constraints. The material of the fiber line was modeled as linear elasticity with Young's modulus E = 31075 MPa and Poisson's ratio $v = 0.36$.

4. Experiments and Result Analysis

As shown in Fig. 5, the experimental platform was constructed to test samples of the bending actuator. A micro air pump was used as the gas source, the four-way plastic tube was used to divert the air flow, and three air pressure regulating valves to control the air flow and the electromagnetic

https://doi.org/10.1017/S0263574720001514 Published online by Cambridge University Press

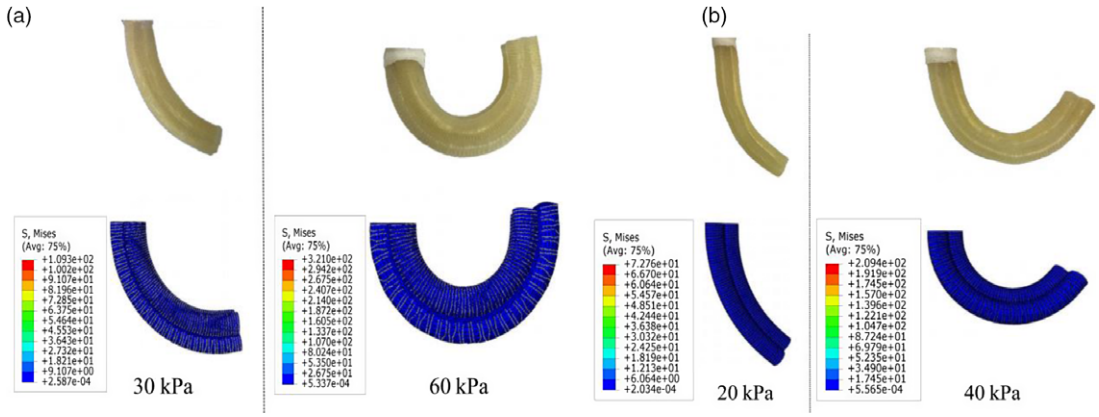

Fig. 6. Bending deformation: (a) single cavity of bending actuator filled with 30 and 60 kPa air pressure; (b) double cavity of bending actuator filled with 30 and 60 kPa air pressure.

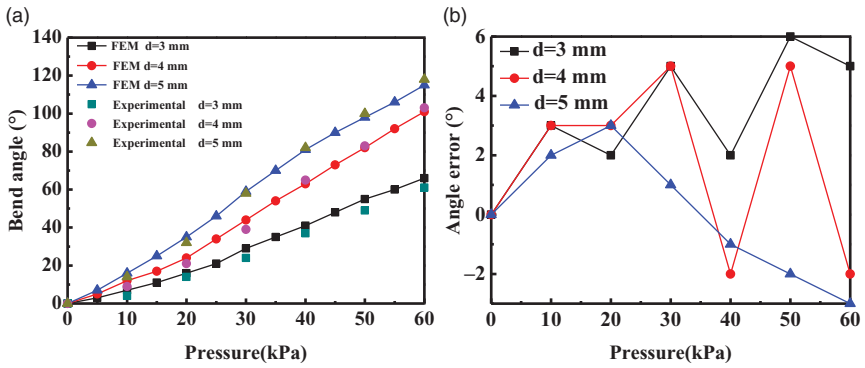

Fig. 7. (a) The bend angle result of the single-cavity inflation of the bending actuator; (b) single-cavity inflation test experimental and simulation result error of the bending actuator.

valve were used to switch the air flow. Each cavity of the actuator is connected to a gas pressure regulating valve and an electromagnetic valve. In the experiment, the actuator is controlled to perform bending, elongation and torsion deformation by driving the cavities. A camera was used to record the deformation of the actuator at different pressures. When testing torsional actuators, the position of the pointer at the front end of the torsional actuator is marked at different air pressures, and then the torsion angle is calculated from the recorded data. In the actual experiment, the measurement average is taken by multiple tests to reduce the measurement error, and the number of experiments is not less than three times.

4.1. Bending and elongation

Soft tubes with inner diameters of 3, 4 and 5 mm were used to investigate the influence of the inner diameter of the soft tube on the performance of the designed bending actuator. The influence of the diameter of the soft tube on the performance of the bending actuator was studied by experimental test and finite element analysis.

4.1.1. Bending actuation. The bending actuator will bend in different directions when its different cavities inflated. The upper cavity of the bending actuator is filled with pressurized air, and the pressure of input air varies from 0 to 60 kPa and increased the air pressure by 5 kPa each time. The bottom soft tube limits the elongation of the upper soft tube, resulting in a bending deformation of the entire bending actuator. Figure 6 shows the bending deformation comparison of the physical and FEMs of the bending actuator at a specific pressure. It can be seen from Figs. 7(b) and 8(b) that the error between the finite element analysis results and the experimental test results is small.

https://doi.org/10.1017/S0263574720001514 Published online by Cambridge University Press

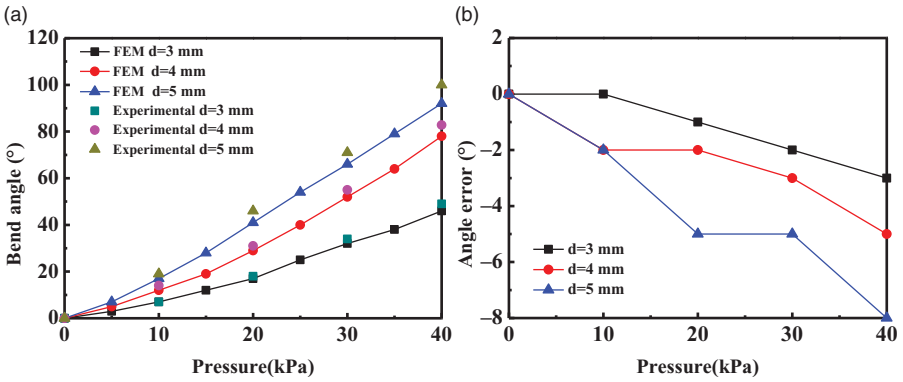

Fig. 8. (a) The bend angle result of the double-cavity inflation of the bending actuator; (b) double-cavity inflation test experimental and simulation result error of the bending actuator.

Figure 7(a) shows the effect of the inner diameter of the soft tube on the bending angle of the bending actuator. As we can see from the figure: (1) for each kind of bending actuator, the bending angle will increase as the input air pressure increases; (2) under the same input air pressure, the bending angle of the bending actuator increases as the diameter of the soft tube increases; this means that if the bending actuators of all kinds are to achieve the same bending angle, bending actuators with a smaller internal cavity diameter require greater air pressure. In the experiment, we found that as the input air pressure increases, the bending angle of the soft actuator with a diameter of 5 mm will be larger, while the radial expansion of the soft tube is more obvious. When the air pressure is further increased, a "balloon" phenomenon will occur, causing damage to the actuator. Based on the above conclusions and phenomena, the bending actuator with an inner diameter of 4 mm is optimum.

The two soft tubes are inflated by the air valve to investigate the effect of the diameter of the soft tube on the bending angle of the bending actuator. The test results are shown in Fig. 8(a): (1) the two soft tubes are inflated at the same time, under the same air pressure, and the bending actuator with a larger inner cavity diameter has a greater bending angle. Compared with Fig. 7 (a), it can be found that: (1) in the pressure range of $0 \sim 10$ kPa, the bending angle of the bending actuator when the single cavity and the double cavity are inflated is basically the same under the same air pressure; (2) within the pressure range of $15 \sim 40$ kPa, the bending angle of the double-cavity inflation of the bending actuator exceeds the bending angle of the single-cavity inflation.

4.1.2. Elongation actuation. Three cavities of the bending actuator are filled with gas at the same time to elongate the actuator, and the length of the actuator elongation is controlled by the input air pressure. A coefficient ε is used to characterize the change in length of the bending actuator during inflated. For this coefficient, it can be defined using formula (1), where l_0 represents the length of the bending actuator when there is no air pressure, and l_1 represents the length of the bending actuator when inflated.

$$\varepsilon = \frac{l_1 - l_0}{l_0} \tag{1}$$

As shown in Fig. 9(d), as the air pressure increases, the elongation of the bending actuator becomes larger as the inner diameter increases. In the range of $20 \sim 25$ kPa and $25 \sim 30$ kPa, there is a decline in the growth rate of the elongation of the soft actuator with a diameter of 5 and 4 mm. The reason for this change is that, the fiber line wound on the surface of the soft tube has a certain spacing; as the input air pressure increases, the soft tube will radially expand at the spacing of the fiber line and even the tiny "balloon" will occur. The soft tube occurs radial elongation beside axial elongation, which causes the increase rate of the overall elongation to decrease. As the input air pressure increases, the axial elongation of the soft tube is much larger than the radial expansion of the soft tube, and the amplitude of the overall elongation of the bending actuator increases again. Since the wall of the bending actuator with an inner diameter of 3 mm is thicker, the soft tube does not have a significant radial expansion during the entire pressurization process, so the increase rate is always increased.

https://doi.org/10.1017/S0263574720001514 Published online by Cambridge University Press

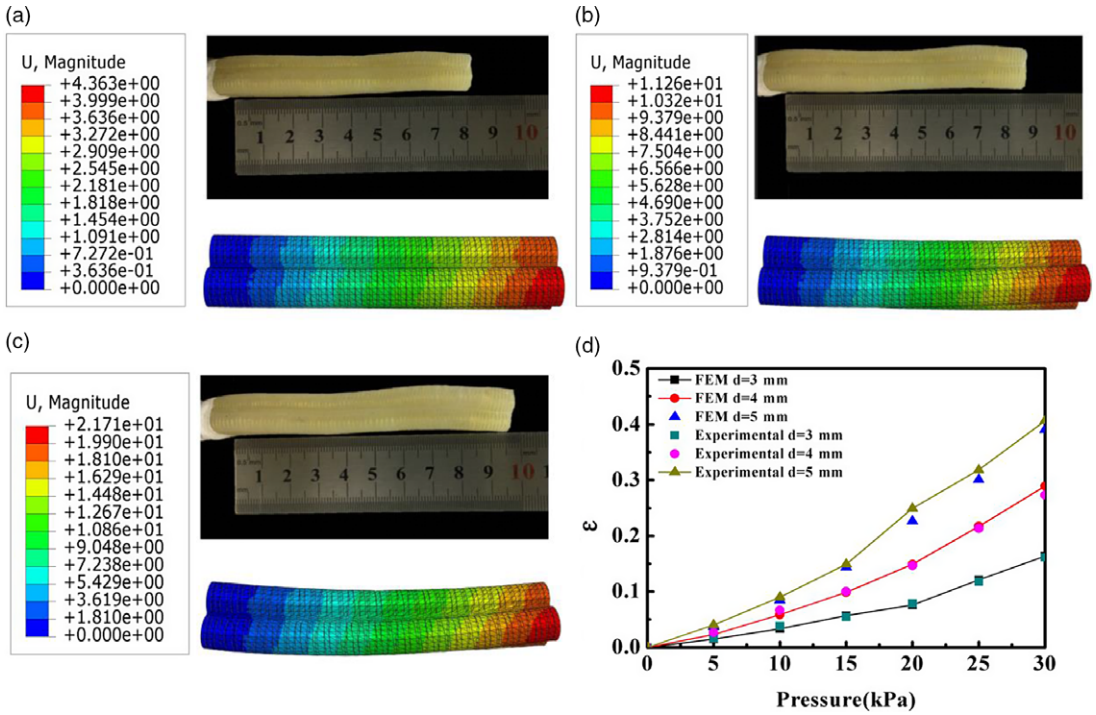

Fig. 9. Bending actuator elongation actuation (d = 4 mm) experimental test (a, b, c) and results (d).

4.2. Torsion actuation

The torsional actuator samples are connected to the experimental test platform. The inner cavity of the soft tube is filled with pressurized air through the air pump, so the soft tube generates axial elongation. When the soft tube is wound around the rigid plastic tube, this axial elongation appears as a rotation around the central rigid plastic tube. The torsional actuator's cavity is inflated with a pressure of 0 ∼ 20 kPa, increasing the pressure by 5 kPa each time. In order to measure the torsional angle of the actuator under different air pressures, the angle of the pointer pointing to the circular paper scale was observed and recorded (Fig. 10). The test results are shown in Fig. 11: (1) Three kinds of torsional actuators with different inner diameters, the torsion angle increases as the input air pressure increases. (2) Under the same air pressure, the torsion angle of the torsional actuator with inner diameter of 4 and 5 mm is larger than that the torsional actuator with inner diameter of 3 mm; when the input air pressure exceeds 15 kPa, due to the thin wall, the torsional actuator with a diameter of 5 mm will cause severe radial expansion, and the axial elongation is limited. Therefore, the performance of the torsional actuator is the best when the inner cavity diameter is 4 mm.

After ascertaining the influence of the inner diameter on the torsion angle of the torsional actuator, the relationship between the winding pitch of the soft tube around the rigid plastic tube and the torsional angle of the torsional actuator was explored. Two methods of finite element simulation and experimental testing were used to analyze the actuation performance of the torsional actuator with a winding pitch of 24 and 40 mm. The final result is shown in Fig. 12.

As can be seen from Fig. 12(a), when the input air pressure is 20 kPa, the finite element analysis results do not converge and the final value cannot be obtained. However, the angle has exceeded 120° at the end of the calculation, so it can be determined that the torsional actuator has a torsion angle larger than 120° at this input air pressure. From Fig. 12, we can get: (1) Under the same input air pressure, the torsion angle of torsional actuator with a winding pitch of 24 mm is greater than 40 mm. (2) For the torsional actuator with the same winding pitch, the torsion angle is positively correlated with the diameter of the torsional actuator. Based on Figs. 11(a) and 12, the influence of the winding pitch on the torsion angle is analyzed. When the input air pressure is the same, the torsion angle of the torsional actuator is the largest when the winding pitch is 24 mm. Therefore, the optimal winding pitch of the torsional actuator is 24 mm.

https://doi.org/10.1017/S0263574720001514 Published online by Cambridge University Press

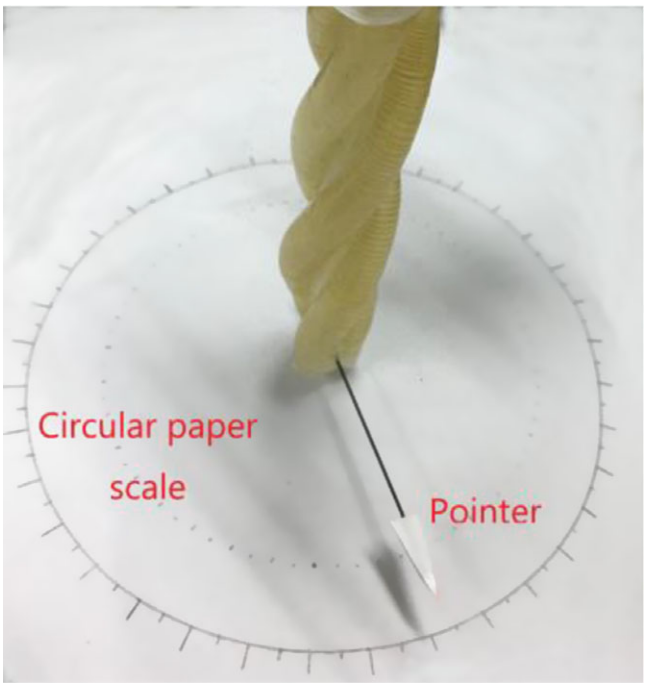

Fig. 10. Experimental test picture of torsional actuator.

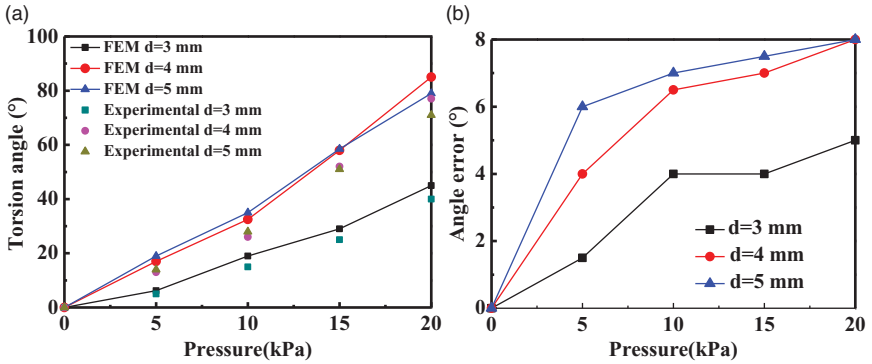

Fig. 11. (a) The torsion angle result of the torsional actuator; (b) experimental and simulation result error of the torsional actuator.

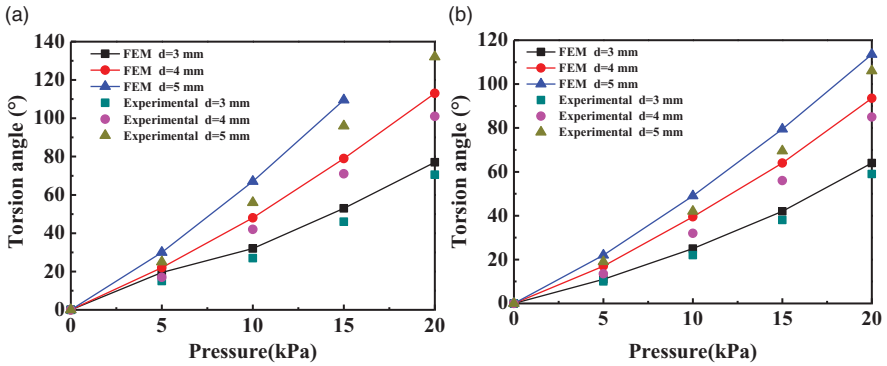

Fig. 12. (a) The torsion angle result of the torsional actuator with a winding pitch of 24 mm; (b) the torsion angle result of the torsional actuator with a winding pitch of 40 mm (b).

https://doi.org/10.1017/S0263574720001514 Published online by Cambridge University Press

Fig. 13. Soft robot arm and soft gripper.

5. Application

For the two pneumatic soft actuators designed, a potential application in the production line is now proposed. As shown in Fig. 13, a soft gripper is made up of three bending actuators, and a soft robot arm is assembled by a torsional actuator and a fixed bracket. The soft gripper can grab lightweight and brittle objects on the production line without any damage to the surface of the objects. The soft robot arm has the function of twisting and it can adjust the angular position of lightweight objects with the soft gripper.

6. Conclusion

Through the multistep process, the soft tube of the basic component is fabricated, and the pneumatic actuator which can perform the bending, torsion and elongation actuation is assembled based on the basic component. For different kinds of soft actuators, the influence of the inner cavity diameter on the actuation performance of the soft actuator is ascertained. The FEM analysis results are compared with the experimental test data, which proves that the model can be used to predict the behavior of soft actuators based on superelastic materials.

For the bending performance of the bending actuator, the actuator has the best bending performance when the inner diameter is 4 mm. When the single cavity is inflated, it has a bending angle of 0–100° in the air pressure range of 0–6 kPa; when the double cavity is inflated and the air pressure is 40 kPa, the bending angle can reach 78°. For the torsion performance of the torsional actuator, when the inner diameter is 4 mm and the winding pitch is 24 mm, the torsional performance of the actuator is the best.

The assembly experiments of the two soft actuators show that the bending actuator and the torsional actuator have great application potential in the production line. At the same time, future research on the soft actuators includes solving the "balloon" problem that occurs under high input air pressure, assembling more robot systems and developing more practical applications of soft actuators.

References

1. Y. Cao, J. Z. Shang, K. S. Liang, D. P. Fan, D. X. Ma and L. Tang, "Review of soft-bodied robots," *Chin. J. Mech. Eng*. **48**(3), 25–33 (2012).
2. L. Shi, S. Guo, M. Li, S. Mao, N. Xiao, B. Gao, Z. Song and K. Asaka, "A novel soft biomimetic microrobot with two motion attitudes," *Sensors* **12**(12), 16732 (2012).
3. T. Li, G. Li, Y. Liang, T. Cheng, J. Dai, X. Yang, B. Liu, Z. Zeng, Z. Huang, Y. Luo, T. Xie and W. Yang, "Fast-moving soft electronic fish," *Sci. Adv*. **3**(4), e1602045 (2017).
4. F. B. Zhu, C. L. Zhang, J. Qian, and W. Q. Chen, "Mechanics of dielectric elastomers: materials, structures, and devices,"*J. Zhejiang Univ. Sci. A: Appl. Phys. Eng*. **17**(1), 1–21 (2016).
5. C. Zheng, "A review on robotic fish enabled by ionic polymer–metal composite artificial muscles," *Robot. Biomim*. **4**(1), 24 (2017).

https://doi.org/10.1017/S0263574720001514 Published online by Cambridge University Press

6. J. O. Alcaide, L. Pearson and M. E. Rentschler, "Design, modeling and control of a SMA-actuated biomimetic robot with novel functional skin," *IEEE International Conference on Robotics & Automation*. IEEE, 2017.
7. L. Zhang, M. Xu and H. Yang, "Research on soft manipulator actuated by shape memory alloy (SMA) springs," *2017 IEEE International Conference on Real-time Computing and Robotics (RCAR)*. IEEE, 2017.
8. H. Lee, C. Xia and N. X. Fang,"First jump of microgel: actuation speed enhancement by elastic instability," *Soft Matter* **6**(18), 4342–4345 (2010).
9. T. Nishida, Y. Okatani and K. Tadakuma, "Development of universal robot gripper using MRα fluid," *2014 Joint 7th International Conference on Soft Computing and Intelligent Systems (SCIS) and 15th International Symposium on Advanced Intelligent Systems (ISIS)* (IEEE, 2015).
10. N. W. Bartlett, M. T. Tolley, J. T. Overvelde, J. C. Weaver, B. Mosadegh, K. Bertoldi, G. M. Whitesides and R. J. Wood, "A 3D-printed, functionally graded soft robot powered by combustion," *Science* **349**(6244), 161–165 (2015).
11. R. F. Shepherd, A. A. Stokes, F. Jacob, J. Barber, P. W. Snyder, A. D. Mazzeo, L. Cademartiri, S. A. Morin and G. M. Whitesides, "Using explosions to power a soft robot," *Angew. Chem.* **52**(10), 2892–2896 (2013).
12. F. Ilievski, A. D. Mazzeo, R. F. Shepherd, X. Chen and G. M. Whitesides, "Soft robotics for chemists," *Angew. Chem.* **123**(8), 1930–1935 (2015).
13. R. F. Shepherd, F. Ilievski, W. Choi, S. A. Morin, A. A. Stokes, A. D. Mazzeo, X. Chen, M. Wang and G. M. Whitesides, "Multigait soft robot [Chemistry]," *Proc. Natl. Acad. Sci.* **108**(51), 20400–20403 (2011).
14. P. Panagiotis, L. Stacey, W. Zheng, L. F. Nicolini, B. Mosadegh, G. M. Whitesides and C. J. Walsh, "Towards a soft pneumatic glove for hand rehabilitation," *IEEE International Conference on Intelligent Robots & Systems*. IEEE, 2013.
15. G. Bao, L. Chen, Y. Zhang, S. Cai, F. Xu, Q. Yang and L. Zhang, "Trunk-like soft actuator: design, modeling, and experiments," *Robotica* **38**(4), 732–746 (2020).
16. F. Connolly, C. J. Walsh, K. Bertoldi, "Automatic design of fiber-reinforced soft actuators for trajectory matching," *Proc. Natl. Acad. Sci.* **114**(1): 51–56 (2017).
17. H. K. Yap, H. Y. Ng, and C. H. Yeow, "High-force soft printable pneumatics for soft robotic applications," *Soft Robot.* **3**(3): 144–158 (2016).
18. S. Yi, S. S. Yun and J. Paik, "Characterization of silicone rubber based soft pneumatic actuators," *IEEE/RSJ International Conference on Intelligent Robots & Systems*. 2013.
19. R. V. Martinez, C. R. Fish, X. Chen and G. M. Whitesides, "Elastomeric origami: programmable paper-elastomer composites as pneumatic actuators," *Adv. Funct. Mater.* **22**(7), 1376–384 (2012).
20. J. M. Florez, B. Shih, Y. Bai and J. K. Paik, "Soft pneumatic actuators for legged locomotion," *IEEE International Conference on Robotics & Biomimetics*. 2015.
21. A. D. Marchese, C. D. Onal, D. Rus. "Autonomous soft robotic fish capable of escape maneuvers using fluidic elastomer actuators." *Soft Robot.* **1**(1): 75–84 (2014).
22. Z. Tang, J. Lu, Z. Wang, G. Ma, W. Chen and H. Feng, "Development of a new multi-cavity pneumatic-driven earthworm-like soft robot," *Robotica* **38**(12), 2290–2304 (2020).
23. S. W. Kwok, S. A. Morin, B. Mosadegh, J.-H. So, R. F. Shepherd, R. V. Martinez, B. Smith, F. C. Simeone, A. A. Stokes and G. M. Whitesides, "Magnetic assembly of soft robots with hard components," *Adv. Funct. Mater.* **24**(15), 2180–2187 (2014).
24. M. Cianchetti, T. Ranzani, G. Gerboni, T. Nanayakkara, K. Althoefer and P. Dasgupta, "Soft robotics technologies to address shortcomings in today's minimally invasive surgery: the STIFF-FLOP approach," *Soft Robot.* **1**(2), 122–131.
25. J. M. Florez, M. Shah, M. E. Martin, S. Wurth, L. Baud, J. V. Zitzewitz, R. Brand, S. Micera, G. Courtine and J. Paik, "Rehabilitative soft exoskeleton for rodents," *IEEE Trans. Neural. Syst. Rehabil. Eng.* **25**(2), 107–118 (2017).
26. P. Polygerinos, Z. Wang, K. C. Galloway, R. J. Wood and C. J. Walsh, "Soft robotic glove for combined assistance and at-home rehabilitation," *Robot. Auton. Syst*. **73**(C), 135–143 (2014).

https://doi.org/10.1017/S0263574720001514 Published online by Cambridge University Press